PERFORMANCE ANALYSIS OF VERTICAL UNDERWATER VISIBLE LIGHT COMMUNICATION LINKS

A Thesis

by

Anıl Yılmaz

Submitted to the

Graduate School of Sciences and Engineering
In Partial Fulfillment of the Requirements for
the Degree of

Master of Science

in the
Department of Electrical and Electronics Engineering

Özyeğin University
July 2018

PERFORMANCE ANALYSIS OF VERTICAL UNDERWATER VISIBLE LIGHT COMMUNICATION LINKS

Approved by:

Professor Murat Uysal, Advisor,
Department of Electrical and
Electronics Engineering
Özyeğin University

Assistant Professor Kadir Durak,
Department of Electrical and
Electronics Engineering
Özyeğin University

Assistant Professor Ferkan Yılmaz,
Computer Engineering Department
Yıldız Technical University

Date Approved: 25 July 2018

This thesis is dedicated to my mother, father, and the love of my life, for their love and continuous support

ABSTRACT

Demand for high-bandwidth underwater applications such as image and real-time video transmission, has been increasing parallel to the increase in maritime activities such as environment monitoring, navigation, ocean-pollution control, tactical surveillance, oil and gas field exploration, and coastal security. To satisfy this demand, underwater visible light communication (UVLC) has emerged as a high-capacity alternative to acoustic and RF signaling. One of the major impairments in UVLC systems is turbulence-induced fading as a result of temporal variations in temperature and salinity. Furthermore, unlike the horizontal links modeled with fixed turbulence strength, vertical links experience varying turbulence strength based on the depth-dependent temperature and salinity profiles. In this thesis, we consider a multiple-input multiple-output (MIMO) UVLC link over a vertical turbulence channel, which is modeled as the concatenation of multiple layers. Under the assumption of cascaded log-normal channel model, we derive the outage probability of vertical MIMO UVLC links and provide a quantitative analysis for the diversity gain in terms of the number of transmitter/receivers.

ÖZETÇE

Çevre izleme, navigasyon, okyanus kirliliği kontrolü, taktiksel izleme, petrol ve gaz yatağı keşfi, ve kıyı güvenliği gibi deniz aktivitelerinin artmasına paralel olarak, gerçek zamanlı imge ve görüntü iletimi gibi yüksek bantgenişliği gerektiren sualtı uygulamalara olan talep de artmaktadır. Bu talebi karşılama konusunda, sualtı görüntülü ışık haberleşmesi (underwater visible light communication, UVLC), akustik ve RF haberleşmeye yüksek kapasiteli bir alternatif olarak ortaya çıkmıştır. UVLC sistemlerindeki en önemli sorunlardan biri, sıcaklık ve tuzluluktaki anlık değişimlerden kaynaklanan türbülans kaynaklı sönümlenmedir. Dahası, sabit türbülans gücü ile modellenen yatay bağların aksine, dikey bağlar derinliğe bağlı olan sıcaklık ve tuzluluk profillerine dayalı olarak değişken türbülansa maruz kalır. Bu tezde, birden fazla ardışık katman olarak modellenen dikey bir türbülans kanalı üzerinde çoklu-giriş çoklu-çıkış (multiple-input multiple-output, MIMO) bir UVLC sistemi ele aldık. Basamaklanmış log-normal kanal modeli varsayımı ile dikey MIMO UVLC bağlarının kesinti olasılıklarını çıkardık ve alıcı/verici sayısı cinsinden çeşitlilik kazancının nicel bir analizini sunduk.

ACKNOWLEDGMENTS

Foremost, I am truly thankful to my supervisor, Professor Murat Uysal, for his guidance and mentorship through my M.Sc. studies.

I would like to thank my colleagues Mohammed Elamassie, Farshad Miramirkhani, Hatef Nouri, Mohammad Sadeghi and Mehdi Karbalayghareh for their academic support and rewarding friendship.

I have sincere gratitude to my colleague and friend Burak Kebapci for his crucial help on making this thesis possible.

I would also like to express my gratitude to my friends Botan Citil, Ayberk Bilgin and Ezgi Yurtsever for their moral support and friendship.

I have to thank my girlfriend, Nazli, for her continuous support and love, which helped me keep proceeding during this process.

Finally, a very special word of thanks goes for my beloved parents, Gulsen and Deniz, for their endless love and support throughout my whole life.

TABLE OF CONTENTS

LIST OF TABLES

LIST OF FIGURES

CHAPTER I

INTRODUCTION

Optical Wireless Communication (OWC) refers to a type of optical communication where the laser diodes (LDs) or light emitting diodes (LEDs) are used for the unguided transmission of signals carried by visible light (VL), infrared (IR), or ultraviolet (UV) light [1, 2]. It has gained considerable attention over the last years, due to its high bandwidth, unregulated spectrum and low cost. Where LEDs or lasers are the possible choices for transmission in OWC, photodetectors (PDs) are utilized for the reception of optical signals, similar to fiber-optic communications. OWC systems are mostly based on intensity-modulation/direct-detection (IM/DD), as photodetectors sense the intensity of received optical signals [2].

There has been a requirement for communication in underwater environments since humans started to explore the oceans and many maritime activities emerged as a result. These maritime activities include underwater environment monitoring, navigation, ocean-pollution control, tactical surveillance, oil and gas field exploration, coastal security and such [3]. As there are this many maritime activities that humans show interest to, and the two thirds of earth surface is covered with water, there is a need for scientific development in certain areas that would support this effort of humanity. One such field is underwater wireless communications, as it is cruicial to transfer data in underwater environments because many maritime activities involve data collection from the environment.

Optical wireless communication through underwater environments is refered to as Underwater OWC (UOWC) [4]. When the transmitted signals are in the visible light spectrum, it is referred to as underwater visible light communication (UVLC).

One of the technologies that has been used to enable the wireless communication in underwater environments is the RF transmission [3]. The main advantage that RF offers for underwater wireless communication, is that the RF waves are relatively more tolerant to underwater turbulence [5]. This is an important benefit of RF communication, as the underwater turbulence is one of the major performance degrading factors in the underwater medium. Another advantage of RF transmission in underwater medium is that the RF waves get much less effected by the transitions from a medium to another (e.g. from water to air). This enables a wider range of possible applications involving underwater environments, such as information transfer from an underwater node to an aerial device. On the other hand, the main disadvantage of underwater RF communications is the shorter link range. Since the salt in the seawater creates a conductive transmission medium for the RF waves, the wave propagation is limited to few meters at extra-low frequencies (i.e. 30 – 300 Hz) [6]. Moreover, for these short ranges, very large antennas, high transmission power and costly transceivers are required.

A more popular technology for underwater wireless communication has been the underwater acoustic communication (UWAC). Acoustic communication has emerged as a dominant technology for underwater wireless transmission, with the extensive increase in military applications during the two World Wars. It has been favoured due to its capability of long distance transmission of several tens of kilometers [7]. The reason for the acoustic communication providing a longer transmission range is that, the other transmission technologies suffer more severe attenuation in underwater medium

compared to the acoustic waves. However, an important disadvantage that the acoustic communication has, is the relatively low data rates (i.e. on the order of Kbps) [8]. As the typical frequencies used in underwater acoustic communication are on the orders of KHz, acoustic communication generally cannot exceed the data rates of Kbps. Another disadvantage of the acoustic communication is the severe communication delay. As the propagation speed of sound waves in water is relatively slow (i.e. about 1500 m/s for pure water at 20 Celcius), acoustic transmission suffers from communication delays on the order of seconds [4].

Optical communication has been gaining a considerable attention in the recent years as a possible candidate for underwater wireless communication. Deploying optical systems for communication has been more prevalent for terrestrial communication (e.g. free space optical – FSO communication) due to the lack of scientific knowledge on aquatic optics [4]. This started to change in early 1960s. With the discovery made by Duntley, it has been understood that it was possible to transmit optical signals underwater, with certain wavelengths (i.e. 450 nm – 550 nm) that correspond to blue and green light, which experience relatively lower attenuation than the other wavelengths on the visible light spectrum [9]. Gilbert *et al.* verified his findings experimentally in [10]. This discovery paved the way to the development of early underwater optical communication systems, mainly for military applications. Until the early 2010s, its applications remained mostly in the military area. First commercial optical wireless systems for underwater communication emerged at this time (e.g. BlueComm [11], Amblaux [12], etc.). With the increase in oceanic exploration, the concept of underwater wireless sensor networks (UWSN) is proposed. UWSN comprise many distributed nodes such as autonomous underwater vehicles, seabed sensors and various underwater exploration devices, which communicate with each other to conduct

collaborative underwater exploration. Emergence of this concept lead to an increase in commercial interest for UOWC, hence a parallel increase in the research interest for the area [4].

When we compare the optical transmission with RF signaling in underwater environment, the major distinction that comes forward is how the medium is perceived by the signal carrying waves. Optical waves perceive the underwater environment as dielectric, where the RF waves perceive it as conductor [3]. As the electromagnetic waves suffer from attenuation more in a conductor medium then in a dielectric one, this difference of medium effect generates an advantage of optical transmission over underwater RF communication. This phenomenon makes optical transmission inherently more resistant to attenuation than RF in underwater medium, and results in higher data rate and transmission range being the prominent stronger points for optical communication over RF signaling.

One of the two major disadvantages of acoustic communication over optical, is the lower data rates. As discussed before, the typical carrier frequencies for acoustic transmission are limited up to hundreds of KHz, where the carrier frequencies for optical signals are at the THz level. This creates a potentially huge difference of transmission rates between the two technologies. The second major disadvantage that acoustic communication has against underwater optical wireless communication is the much higher communication delay. Propagation speed of light in underwater is much higher than the propagation speed of sound. This results in a large difference between the communication delays of acoustic and optical systems. In practical perspective, this prohibits some applications for acoustic communication systems to support, that optical communication can provide (e.g. real-time video/audio streaming). Another downside

of acoustic communication that is shared with RF against optical communication in underwater is the implementation of transceivers being costly and less practical.

Because of the aforementioned reasons, UVLC is an interesting area of investigation for the realization of underwater wireless communications, hence the focus of this thesis.

1.1 Fundamentals of VLC

VLC is a communication technology in which, the LEDs or laser diodes are employed for transmitting visible light signals (390 – 750 nm) and photodetectors are employed for their reception. Although the LDs provide a higher intensity and narrower power spectrum, LEDs are generally preferred for the realization of VLC systems, as they have longer lifetime and lower cost. A generic block diagram of a VLC system is shown in Figure 1.

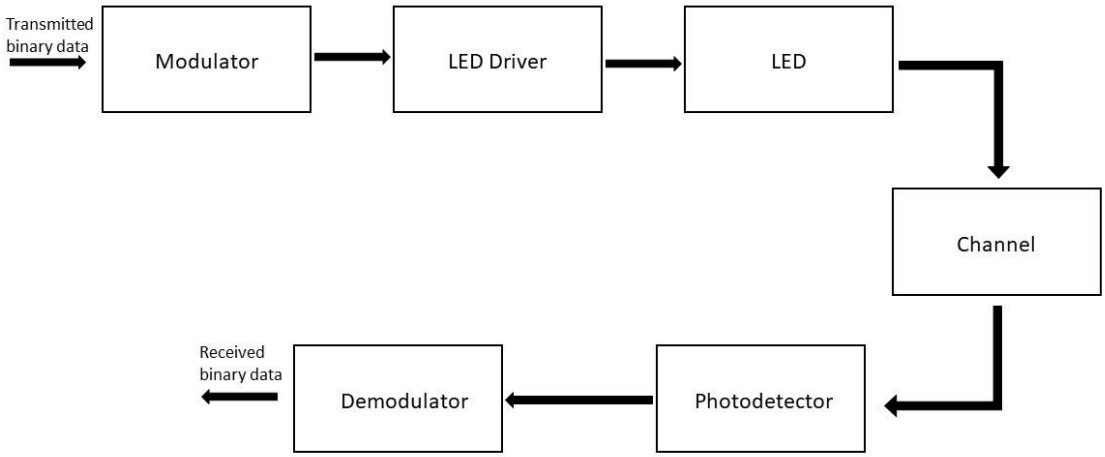

Figure 1: VLC System Block Diagram

In a VLC system, binary data to be transmitted are modulated and passed to the LED Driver, which is a circuitry that drives the LED by supplying current. In the LED

Driver, the AC current from Modulator is coupled with a DC current required to drive the LED. This current drives the LED and results in the transmission of visible light signals, carrying the modulated symbols. A photodetector at the receiver collects photons from the received light and generates proportional electrical current, which is passed into the demodulator to extract the transmitted bits. There are usually an optical filter and a lens to concentrate the diffused light on to the photodetector.

While there are many studies for OWC focusing on the outdoor settings, like the vehicular communication [13] or FSO, general direction of research interest for VLC concentrates on indoor applications [14]. One of the main reasons for this, is the existing backbone infrastructure. It is appealing to have established power lines for illumination, which can be utilized for communication with slight modifications. Another factor that motivates the focus of attention is the increasing popularity of white LEDs as a choice for indoor illumination. It has lower power consumption, faster response, longer lifetime and lower cost than the other lighting devices such as fluorescent lamp or incandescent light bulbs. LEDs are also a preferable physical front-end choice for communication, as they provide a high modulation bandwidth of up to hundreds of MHz [14].

There are currently two different methods to obtain white LEDs [14]. One method is to combine three LEDs with colors red, green, and blue in appropriate proportions to create white light. The other method is to use a blue LED with a phosphor coating that results in white light. While the phosphor coating method is more preferable for illumination due to its lower cost, the method of combining three LEDs is more appealing for telecommunication purposes, as it provides higher modulation bandwidth [14].

1.1.1 Intensity Modulation/Direct Detection (IM/DD)

In RF communications, the receivers are coherent, which means the received signal is down-converted using a local oscillator and a frequency mixer, and the frequency or phase of the received signal can be detected [14]. Similarly, optical coherent receivers detect the optical phase of coherent optical signals (i.e. transmitted by Laser Diodes) in optical communication. However, when we consider LEDs, the transmitted light is incoherent. Therefore, there cannot be enough power for detection when a coherent receiver is used, as it can only detect a very small portion (i.e. a single frequency component) of the transmitted signal.

Even for laser-based systems, which can be developed using coherent receivers, the low cost and simplicity of photodetectors motivate the preference of incoherent detection. This issue motivates intensity modulation and direct detection (IM/DD) to be considered for modulation and demodulation in VLC systems. In intensity modulation, the desired signal is modulated into the intensity of transmitted light. As the sources produce light with the intensity proportional to the input current, this type of modulation is realized by modulating the signals in electrical domain and feeding that electrical signals into the light producing element. Intensity modulated signals are detected with direct detection, in which the instantaneous received optical power is detected by a photodetector, as the photodetector produces electric current proportional to the received optical power. IM/DD enforces a constraint for the modulated signals. As the emitted light signal cannot have imaginary and negative parts, the modulated signals have to be real and non-negative.

For the modulation schemes to be used in electrical domain, there have been several popular options. On-Off Keying (OOK), Pulse-Position Modulation (PPM), and

Pulse-Amplitude Modulation (PAM) are the most preferred single carrier schemes in VLC, due to their easy implementation. There are also multiple carrier schemes for VLC. Mainly, orthogonal frequency division multiplexing (OFDM) has been altered to achieve the real and non-negative signaling requirement of intensity modulation. Two of the dominant OFDM schemes for VLC are DC biased optical OFDM (DCO-OFDM) and asymmetrically clipped optical OFDM (ACO-OFDM) [15].

1.2 Underwater VLC

As any communication system, transmission medium imposes a number of impairments to the signals that are being transmitted, related with its specific characteristics. In underwater VLC, water affects the optical signals in certain ways. Mainly, the optical signals experience attenuation due to absorption and scattering, and fading due to underwater turbulence.

Absorption and scattering are due to the interaction of photons with the underwater particles and microorganisms [16]. Absorption causes the photons to lose their energy by interaction with particles. Hence, some portion of transmitted optical power is lost in the channel. Severity of the absorption being experienced by the optical signal depends on the amount of particles that photons can interact with in the water. Optical signals experience scattering when the photons collide with particles and get deflected from its original path. This causes some photons that originally headed towards the photodetector to be deflected and not reach the receiver.

To model the effects of absoption and scattering, Beer-Lambert's Law [17] is utilized to express this attenuation by

$$P = P_t e^{-c(\lambda)d} \tag{1}$$

where P_t is the transmitted optical power, $c(\lambda)$ is the extinction coefficient as a function of wavelength λ, composed of absorption and scattering coefficients, and P is the optical power after traveling a distance of d.

A different model, which uses two exponentials to model the attenuation is also proposed [18]. This model approximates the channel power loss for long distances more accurately than the Beer-Lambert's model, however the model parameters are obtained by data fitting to simulation data, hence not providing a general analytical expression.

An improvement on the Beer-Lambert model is proposed in [19], which includes the geometric loss in the calculation and provides a better accuracy than the model expressed in (1), in modeling the underwater path loss.

Besides these analytical modeling approaches, there have also been numerical methods proposed, in which the channel impulse responses (CIR) for specific underwater environments obtained by ray tracing simulations [18, 20-25]. Numerical models are useful to evaluate specific settings, though they do not provide insights that have generic use.

As mentioned before, another major channel effect on the optical signals is the fading caused by underwater turbulence. Turbulence is the phenomenon that causes instantaneous changes on refractive index of the water [4]. Turbulence occurs because of the instantaneous variations of the density, caused by the rapid changes of temperature, salinity and pressure.

These changes of refractive index cause instantaneous variations on received optical power. Therefore, turbulence-induced fading manifests itself as a multiplicative fading coefficient which can be modeled as a random variable. Several studies adopted

the log-normal turbulence model from free space optical communication, which is used for modeling the atmospheric turbulence [26-38]. Statistical distribution of the fading coefficient was experimentally evaluated in [39] and [40], and it was proposed that the log-normal distribution for the weak turbulence and Gamma-Gamma distribution for the strong turbulence accurately model the random fluctiations. In [41], the statistical distribution of optical intensity fluctuations is also investigated experimentally and it is suggested that the generalized Gamma distribution (GGD) precisely fits the measured data. However, parameters of GGD are computed from the measured data and dependent to the specific setting. Hence, it does not provide a general model whose parameters can be obtained from the channel.

In the studies that consider the effect of turbulence-induced fading in the channel model [26-38, 42], the considered model for turbulence is the log-normal turbulence model, given as

$$f_{\alpha}(\alpha) = \frac{1}{\alpha\sqrt{2\pi 4\sigma_X^2}} \exp\left(-\frac{\left(\ln(\alpha) - 2\mu_X\right)^2}{2\left(4\sigma_X^2\right)} \right) \tag{2}$$

where α is the multiplicative fading coefficient, and μ_X and σ_X^2 denote the mean and variance of the log-amplitude coefficient $X = 0.5\ln(\alpha)$. Figure 2 below shows the log-normal PDFs with different log-amplitude variances.

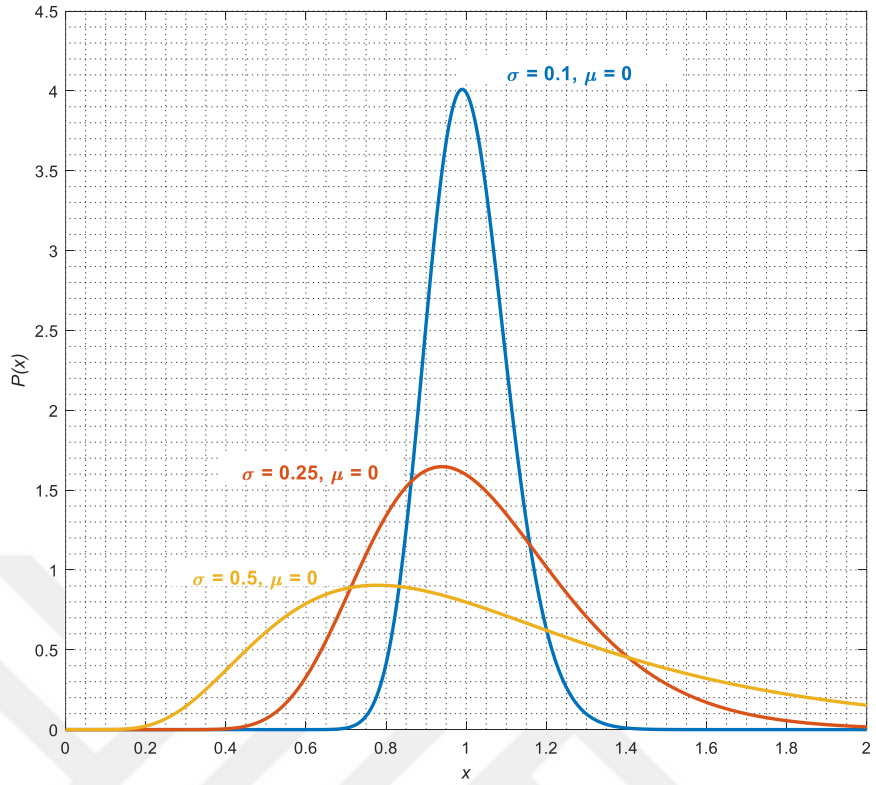

Figure 2: Log-normal PDF

When considering the log-normal turbulence model, to ensure that the multiplicative fading coefficient does not affect the average received power, the fading amplitude is normalized such that $E[\alpha]=1$, which is satisfied by $\mu_X=-\sigma_X^2$. Here, the log-amplitude is the only parameter needed to model the turbulence and it can be computed via its relation with scintillation index σ_Y^2, which is expressed as

$$\sigma_X^2=0.25\ln\left(1+\sigma_Y^2\right) \tag{3}$$

Scintillation index is a quantitative measure for strength of optical intensity fluctuation, and it can be obtained by [43]

$$\sigma_Y^2=8\pi^2k_0^2d\int_0^1\int_0^\infty \kappa\Phi_n(\kappa)\times\left\{1-\cos\left[\frac{d\kappa^2}{k_0}\zeta\left(1-\left(1-\Theta\right)\zeta\right)\right]\right\}d\kappa d\zeta \tag{4}$$

where d is the travelling distance of the signal, λ is the wavelength, $k_0 = 2\pi/\lambda$ is the wave number, and the wave type selector $\Theta = 1$ or 0 for plane and spherical waves, respectively. $\Phi_n(\kappa)$ is the spatial power spectrum model of turbulent fluctuations of the sea-water refraction index and given by [16]

$$\Phi_n(\kappa) = \left(4\pi\kappa^2\right)^{-1} C_0 \left(\frac{A^2 \chi_T}{\omega^2}\right) \varepsilon^{-1/3} \kappa^{-5/3} \left[1 + C_1 (\kappa\eta)^{2/3}\right] \times \left[\omega^2 \exp\left(-C_0 C_1^{-2} P_T^{-1} \delta\right) + d_r \exp\left(-C_0 C_1^{-2} P_S^{-1} \delta\right) - \omega(d_r + 1) \exp\left(-0.5 C_0 C_1^{-2} P_{TS}^{-1} \delta\right)\right] \tag{5}$$

where δ and d_r are defined as

$$\delta = 1.5 C_1^2 (\kappa\eta)^{\frac{4}{3}} + C_1^3 (\kappa\eta)^2 \tag{5.a}$$

$$d_r \approx \begin{cases} |\omega| \Big/ \left(|\omega| - \sqrt{|\omega|\left(|\omega| - 1\right)}\right), & |\omega| \geq 1 \\ 1.85|\omega| - 0.85, & 0.5 \leq |\omega| \leq 1 \\ 0.15|\omega|. & |\omega| < 0.5 \end{cases} \tag{5.b}$$

Definitions of the variables in (4) and (5) are provided in Table I.

TABLE I. Definition of variables in (4) and (5)

Parameter	Definition
λ	Wavelength
$k_0 = 2\pi / \lambda$	Wave number
κ	Magnitude of the spatial frequency
ε	Dissipation rate of turbulent kinetic energy per unit mass of fluid
χ_T	Dissipation rate of mean-squared temperature
C_0 =0.72	Constant
C_1 =2.35	Constant
A	Thermal expansion coefficient
B	Saline (i.e., Haline) contraction coefficient.
$\eta = \left(\upsilon^3 / \varepsilon\right)^{1/4}$	Kolmogorov microscale length
$\left(dT_0 / dz\right)$	Temperature differences between top and bottom boundaries
$\left(dS_0 / dz\right)$	Salinity differences between top and bottom boundaries
υ	kinematic viscosity
D_T	Molecular diffusivity of temperature
$D_S \approx 0.01 D_T$	Molecular diffusivity salinity
$\omega = \frac{A\left(dT_0 / dz\right)}{B\left(dS_0 / dz\right)}$	Relative strength of temperature and salinity fluctuations
$P_T = \upsilon D_T^{-1}$	Prandtl number for temperature
$P_S = \upsilon D_S^{-1}$	Prandtl number for salinity
P_{TS}	One-half of the harmonic mean of P_T and P_S

In [42] it was argued that, as the scintillation index depends on the temperature and salinity values, the turbulence strength changes with depth, due to the dependence of temperature and salinity to depth. Changes of temperature and salinity with depth are shown in Figure 3.

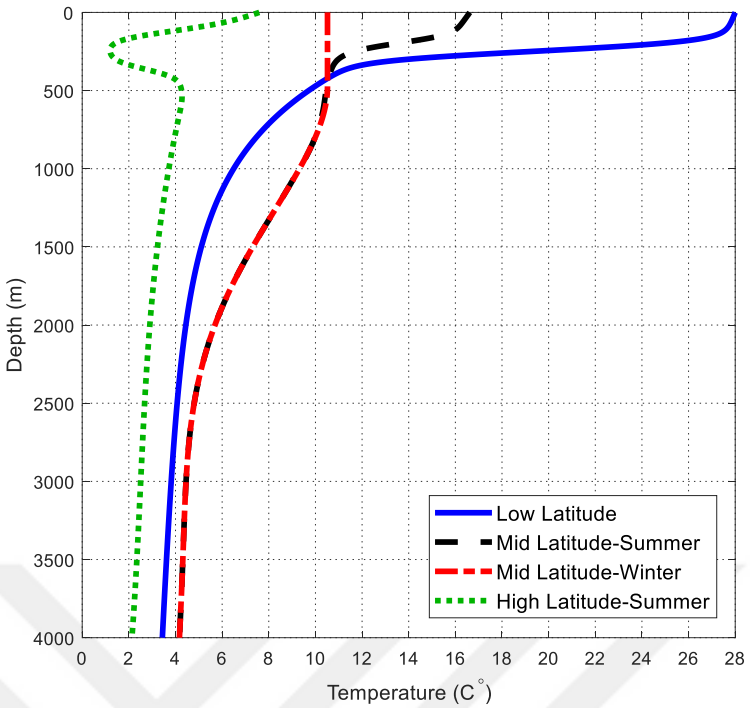

(a)

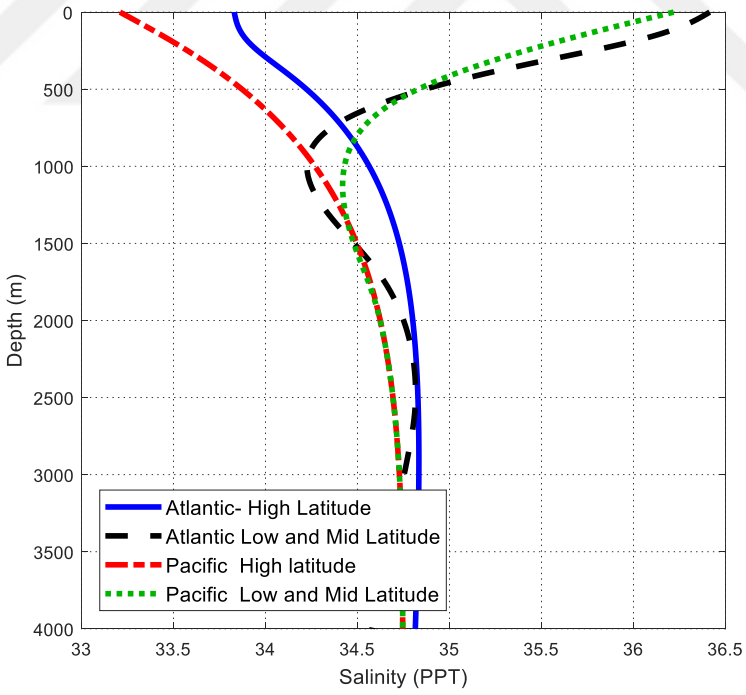

(b)

Figure 3: Oceanic profiles: (a) Temperature (b) Salinity

Therefore, it was suggested in [42] that, when a vertical link between the transmitter and the receiver is considered, a constant strength turbulence model is misleading. Hence, a model for vertical transmission, which composes of cascaded independent turbulence layers, each having a different scintillation index $\sigma_{Y_k}^2$ was proposed as

$$f_\alpha(\alpha) = \frac{1}{\alpha\sqrt{2\pi 4\sum_{k=1}^{K}\sigma_k^2}} \exp\left(-\frac{\left(\ln(\alpha) - 2\sum_{k=1}^{K}\mu_k\right)^2}{8\sum_{k=1}^{K}\sigma_k^2} \right) \tag{6}$$

where μ_k and σ_k^2 denote the mean and variance of log-amplitude coefficient of the k^{th} layer and *K* denotes the total number of layers.

1.3 Motivation

The focus of UVLC research had been concentrated on the effects of absorption and scattering and the underwater turbulence had been ignored for a time. For the last several years, turbulence has started to grab attention in the research community. The models proposed for the underwater turbulence still need to be further investigated experimentally, and the understanding of the underwater environment needs to be broadened.

MIMO has been an effective method to combat the harsh effects of fading. MIMO is considered in several studies in the UVLC literature [24, 25, 37, 38]. The focus of these studies are either analyzing the attenuation by extracting the channel impulse responses of specific settings [24, 25], or the performance analysis of MIMO systems [37, 38]. Most studies that consider turbulence, assume a fixed log-amplitude variance for turbulence-induced fading. As pointed out in [42], the log-amplitude

variance of the fading coefficient depends on the temperature and salinity of the water, hence this approach of fixed variance requires the implicit assumption of non-changing temperature and salinity through the link. This may be valid only for horizontally separated transmitter and receiver, i.e. when they are located at the same depth.

To the best of our knowledge, there has not been a quantitative study on analyzing the diversity gain for UVLC systems. In addition, as the major turbulence studies assume horizontal links, in this thesis, we investigate the diversity gain for vertical MIMO UVLC links.

The rest of the thesis is organized as follows: In Chapter 2, we present the system and channel model considered. In Chapter 3, we derive the outage probability and diversity gain for the considered system and present the numerical results. Finally, we conclude in Chapter 4.

CHAPTER II

SYSTEM AND CHANNEL MODEL

2.1 System Model

As illustrated in Figure 4, we consider a MIMO UVLC link with *M* light sources at the transmitter and *N* photodetectors at the receiver. As IM/DD is employed for detection on optical communication, unlike RF, multiple light sources can be utilized to transmit the same signal [44]. This type of utilization of multiple transmit devices is called the Repetition Coding (RC). Also, due to the same characteristics, conventional MIMO techniques for RF can not be directly applied to OWC. An OWC adaptation of the conventional MIMO techniques has been proposed in [45]. However, it has been proven that the best performing MIMO technique for OWC is the RC [46, 47]. Therefore, we adopt the RC technique, in which all the light sources transmit the same symbol, in this thesis.

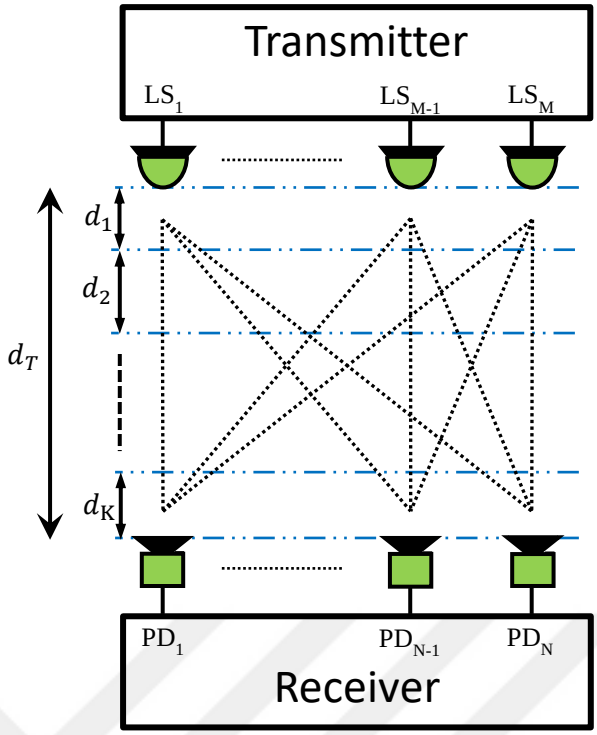

Figure 4: MIMO UVLC system model (LS: Light source, PD: Photodetector)

On the receiver side, we employ Equal Gain Combining (EGC) method, in which the received signal outputs of all antennas (photodetectors in our case) are added up with equal weighting factor.

We assume that all light sources transmit the same modulated symbol, x, with power P_t/M, where P_t is the total optical transmit power. Each light source has this transmit power of P_t/M to have a fair comparison between the systems with different number of light sources at the transmitter. A similar adjustment for fairness is made for the total received optical power, by considering the photodetector areas as A_r/N, where A_r is the area of the photodetector when there is only a single photodetector at the receiver (i.e. MISO/SISO system) [48]. With these considerations, the received signal at the n^{th} photodetector from the m^{th} light source can be written as

$$y_n = \frac{(P_t/M)}{N} R x \sum_{m=1}^{M} \alpha_{m,n} + w_n \quad (7)$$

where R is the photodetector responsivity, and $\alpha_{m,n}$ is the turbulence-induced fading coefficient between the n^{th} photodetector and the m^{th} light source. w_n is the composite noise term. It consists of the thermal noise, shot noise (or photocurrent shot noise), dark current noise and the background noise [48]. Thermal noise caused by, like for any other type of receiver, the electronic circuitry utilized for reception. It is modeled as a zero mean Gaussian process. Shot noise is due to the quantum effects taking place in the photodetector. The amount of generated current when a photon hits the photodetector is probabilistic. This causes some fluctuations on the output current of a photodetector [49]. Dark current noise is caused by the leakage current from the bias voltage of photodiodes. It is modeled as a Gaussian process [49]. Background noise is actually the shot noise caused by not the signal but the ambient background light. We assume this composite noise is dominated by the background noise (i.e. background-limited receiver) and the noise term w_n can be described as additive white Gaussian noise (AWGN), i.e. $w_n \sim N\left(0, \sigma_{w_n}^2\right)$ [48]. As the light sources, as well as photodetectors are separated from each other by a very small distance compared to the transmission range, each link from m^{th} light source to n^{th} photodetector can be safely assumed to have the same length. This allows us to assume the attenuations experienced on each link to be the same, hence the attenuation coefficient is normalized to one, and does not appear on (7).

As mentioned before, we employ EGC at the receiver. Therefore, the combined received signal at the receiver is

$$y_{\mathrm{T}} = \sum_{n=1}^{N} y_n = \frac{\left(P_t / M\right)}{N} R\, x \sum_{n=1}^{N} \sum_{m=1}^{M} \alpha_{m,n} + \sum_{n=1}^{N} w_n \tag{8}$$

As we sum the outputs of N photodetectors, we have the combined noise term $\sum_{n=1}^{N} w_n$ in (8). As we assume the noise is background-limited, the noise variance is proportional to the aperture area size [48]. As the photodetector area sizes are scaled by the number of photodetectors at the receiver (i.e. A_r / N), noise variances of each photodetector are also scaled by the same factor. Therefore, combined noise term, which can be defined as $\sum_{n=1}^{N} w_n = w$ always has the same variance for each different MN setting, i.e. $w \sim N\left(0, \sigma_w^2\right)$ where $\sigma_w^2 = N_0 / 2$ [50].

2.2 Channel Model

As it can be seen from Figure 4, we consider a MIMO system where the transmitter and the receiver are vertically separated, i.e. the communication links are vertical. As we consider a vertical transmission, we adopt the channel model of [42] explained in the first chapter, which is a fading model for vertical underwater links.

The variance of the fading coefficient for each layer is calculated by averaging the temperature and salinity through the thickness of the layer. The average temperature and salinity values for a layer is used to compute the scintillation index of the layer using (4) and (5). The values of temperature and salinity change gradually, so a single average value for a link can be used in a certain region. We model our vertical fading coefficients $\alpha_{m,n}$ using this concept of layers. The layers are shown in Figure 4, each having a thickness of d_k, with $\sum_{k=1}^{K} d_k = d_T$, where d_T is the total transmission range between the transmitter and the receiver. We assume that each layer has an independent

multiplicative fading coefficient $\alpha_{m,n,k}$ where *k* represents the k^{th} layer. As we assume log-normal model for weak turbulence, the probability density function for $\alpha_{m,n,k}$ is [32]

$$f_{\alpha_{m,n,k}}\left(\alpha_{m,n,k}\right)=\frac{1}{\alpha_{m,n,k}\sqrt{2\pi 4\sigma_{m,n,k}^2}}\exp\left(-\frac{\left(\ln\left(\alpha_{m,n}\right)-2\mu_{m,n,k}\right)^2}{2\left(4\sigma_{m,n,k}^2\right)}\right) \tag{9}$$

where $\mu_{m,n,k}$ and $\sigma_{m,n,k}^2$ denote the mean and variance of log-amplitude coefficient $X_{m,n,k}=0.5\ln\left(\alpha_{m,n,k}\right)$ for the fading coefficient associated with layer *k* for link from the m^{th} light source to the n^{th} photodetector. To ensure that the multiplicative fading coefficient does not affect the average received power, the fading amplitude is normalized such that $E\left[\alpha_{m.n.k}\right]=1$, which is satisfied by $\mu_{\mathrm{m,n,k}}=-\sigma_{\mathrm{m,n,k}}^2$. As we assume that the light sources on the transmitter, as well as the photodetectors on the receiver, are separated by a very small distance compared to the transmission range, the traveling distances of signals are assumed to be the same for each layer (i.e. each signal on each link travel d_k on the k^{th} layer). As the traveling distances on a layer are the same for the signals on different links, the fading coefficient associated with a link has the same mean and variance for each link, i.e. $\mu_{m,n,k}=\mu_k$ and $\sigma_{m,n,k}^2=\sigma_k^2$ for every *m* and *n* where μ_k and σ_k^2 denote the mean and variance of log-amplitude coefficient for the layer *k*. Therefore, (9) can be rewritten as

$$f_{\alpha_{m,n,k}}\left(\alpha_{m,n,k}\right)=\frac{1}{\alpha_{m,n,k}\sqrt{2\pi 4\sigma_k^2}}\exp\left(-\frac{\left(\ln\left(\alpha_{m,n,k}\right)-2\mu_k\right)^2}{2\left(4\sigma_k^2\right)}\right) \tag{10}$$

As our vertical channel is comprised of concatenated layers, each with a different fading coefficient $\alpha_{m,n,k}$, the distribution of $\alpha_{m,n}$, the fading coefficient of the composite link between the m^{th} light source and the n^{th} photodetector is

$$f_{\alpha_{m,n}}\left(\alpha_{m,n}\right)=\frac{1}{2\alpha_{m,n}\sqrt{2\pi\sum_{k=1}^{K}\sigma_k^2}}\exp\left(-\frac{\left(\ln\left(\alpha_{m,n}\right)-2\sum_{k=1}^{K}\mu_k\right)^2}{8\sum_{k=1}^{K}\sigma_k^2}\right) \tag{11}$$

as suggested in [42].

CHAPTER III

OUTAGE AND DIVERSITY GAIN ANALYSIS

In this chapter, we provide the diversity gain analysis of the mentioned system. As the performance metric to be used in the analysis, we first obtain the outage probability expression of the system. Then we utilize the outage probability expressions for MIMO and SISO systems to derive a comparative performance metric for diversity gain

3.1 Outage Probability

Outage probability is defined as the probability that the instantaneous received signal-to-noise ratio (SNR) drops below a certain threshold [35]. Mathematically speaking, we have

$$P_{\text{out}} = P\left(\gamma < \gamma_{\text{th}}\right) \tag{12}$$

where γ stands for electrical SNR at the receiver. γ_{th} is the SNR threshold and chosen such that it provides an acceptable error rate performance for the intended application. Based on (8), the total received optical power is

$$P_R = \frac{P_t R}{MN} \sum_{n=1}^{N} \sum_{m=1}^{M} \alpha_{m,n} \tag{13}$$

The electrical SNR can be expressed as

$$\gamma = \frac{P_R^2}{\sigma_w^2} = \frac{\left(\sum_{n=1}^{N}\sum_{m=1}^{M}\alpha_{m,n}\right)^2}{(MN)^2}\underbrace{\frac{R^2P_t^2}{\sigma_w^2}}_{\gamma_0} \tag{14}$$

where γ_0 is the fading-free SNR. When we insert (14) in (12), we obtain the outage probability as

$$P_{\text{out}} = P\left(\frac{\left(\sum_{n=1}^{N}\sum_{m=1}^{M}\alpha_{m,n}\right)^2}{(MN)^2}\gamma_0 < \gamma_{\text{th}}\right) \tag{15}$$

When we rearrange (15), we can obtain

$$P_{\text{out}} = P\left(\sum_{n=1}^{N}\sum_{m=1}^{M}\alpha_{m,n} < (MN)\sqrt{\frac{\gamma_{\text{th}}}{\gamma_0}}\right) \tag{16}$$

Let $P_{\text{M}} = \sqrt{\gamma_0/\gamma_{\text{th}}}$ denote the power margin [51]. Power margin can be expressed as the increase in received power above the threshold received power required to produce no outage (i.e. achieve the desired error probability). Replacing the P_{M} in the formula, our outage probability expression becomes

$$P_{\text{out}} = P\left(\sum_{n=1}^{N}\sum_{m=1}^{M}\alpha_{m,n} < (MN)\frac{1}{P_{\text{M}}}\right) \tag{17}$$

We can approximate the summation of the log-normal variables $\sum_{n=1}^{N}\sum_{m=1}^{M}\alpha_{m,n}$ as another log-normal variable $Z = e^U$, where the log-amplitude U follows a normal distribution, i.e. $U \sim N\left(\mu_U, \sigma_U^2\right)$ [48]. Therefore, the outage probability expression becomes

$$P_{\text{out}} = P\left(Z < (MN)\frac{1}{P_{\text{M}}} \right) \tag{18}$$

The mean μ_U and variance σ_U^2 of the log-amplitude of Z are respectively given by[48]

$$\mu_U = \ln(MN) - \frac{1}{2}\ln\left(1 + \frac{e^{4\sum_{k=1}^{K}\sigma_k^2} - 1}{MN} \right) \tag{19}$$

$$\sigma_U^2 = \ln\left(1 + \frac{e^{4\sum_{k=1}^{K}\sigma_k^2} - 1}{MN} \right) \tag{20}$$

Using the CDF of log-normal distribution, which is expressed as $F_X(x) = P(X \le x) = Q\left(\frac{\ln(1/x) + \mu}{\sigma} \right)$, where μ and σ^2 are the mean and variance of the log-amplitude coefficient for x, we obtain the expression for P_{out} as

$$P_{\text{out}} = Q\left(\frac{\ln(P_{\text{M}}) - 0.5\ln\left(1 + \frac{1}{MN}\left(\exp\left(4\sum_{k=1}^{K}\sigma_k^2 \right) - 1 \right) \right)}{\sqrt{\ln\left(1 + \frac{1}{MN}\left(\exp\left(4\sum_{k=1}^{K}\sigma_k^2 \right) - 1 \right) \right)}} \right) \tag{21}$$

where $Q(x)$ denotes the Gaussian Q function and is given by $Q(x) = \left(1/\sqrt{2\pi}\right)\int_x^{\infty} \exp\left(-u^2/2\right) du$

3.2 Diversity Gain Analysis

Diversity order is conventionally defined as the negative asymptotic slope of the outage probability versus SNR on a log-log scale. The conventional definition of diversity order over log-normal fading channels yields infinity and does not provide a

meaningful measure for diversity gain. To overcome this problem, we adopt relative diversity order (RDO) of [52] to quantify the diversity gain. RDO is defined as [52]

$$RDO\left(P_{\mathrm{M}}\right)=\frac{\partial \ln P_{\mathrm{out}}/\partial \ln P_{\mathrm{M}}}{\partial \ln P_{\mathrm{out,SISO}}/\partial \ln P_{\mathrm{M}}} \tag{22}$$

where $P_{\mathrm{out,SISO}}$ is the outage probability of the benchmarking SISO scheme. Asymptotic relative diversity order (ARDO) is further defined as

$$ARDO=\lim_{P_{\mathrm{M}}\to\infty} RDO\left(P_{\mathrm{M}}\right) \tag{23}$$

When we replace the outage probability expression (21) in (22), we have the RDO expression as

$$RDO\left(P_{\mathrm{M}}\right)=\frac{\partial \ln\left(Q\left(\frac{\ln\left(P_{\mathrm{M}}\right)-0.5\ln\left(1+\frac{1}{MN}\left(\exp\left(4\sum_{k=1}^{K}\sigma_k^2\right)-1\right)\right)}{\sqrt{\ln\left(1+\frac{1}{MN}\left(\exp\left(4\sum_{k=1}^{K}\sigma_k^2\right)-1\right)\right)}}\right)\right)\Big/\partial \ln P_{\mathrm{M}}}{\partial \ln\left(Q\left(\frac{\ln\left(P_{\mathrm{M}}\right)-2\sum_{k=1}^{K}\sigma_k^2}{\sqrt{4\sum_{k=1}^{K}\sigma_k^2}}\right)\right)\Big/\partial \ln P_{\mathrm{M}}} \tag{24}$$

Using the Chernoff bound on Q function, i.e. $Q\left(x\right)\le 0.5\exp\left(-x^2/2\right)$, (24) becomes

$$RDO\left(P_{\mathrm{M}}\right)=\frac{\partial\left(\ln\left(0.5\right)-\frac{\left(\ln\left(P_{\mathrm{M}}\right)-0.5\ln\left(1+\frac{1}{MN}\left(\exp\left(4\sum_{k=1}^{K}\sigma_k^2\right)-1\right)\right)\right)^2}{2\ln\left(1+\frac{1}{MN}\left(\exp\left(4\sum_{k=1}^{K}\sigma_k^2\right)-1\right)\right)}\right)\Big/\partial \ln\left(P_{\mathrm{M}}\right)}{\partial\left(\ln\left(0.5\right)-\frac{\left(\ln\left(P_{\mathrm{M}}\right)-2\sum_{k=1}^{K}\sigma_k^2\right)^2}{8\sum_{k=1}^{K}\sigma_k^2}\right)\Big/\partial \ln\left(P_{\mathrm{M}}\right)} \tag{25}$$

Inserting (25) in (23) and taking the derivative with respect to $\ln\left(P_{\mathrm{M}}\right)$, we have ARDO as

$$ARDO=\lim_{P_{\mathrm{M}}\to\infty}\frac{\left(\ln\left(P_{\mathrm{M}}\right)-0.5\ln\left(1+\frac{1}{MN}\left(\exp\left(4\sum_{k=1}^{K}\sigma_k^2\right)-1\right)\right)\right)\Big/\ln\left(1+\frac{1}{MN}\left(\exp\left(4\sum_{k=1}^{K}\sigma_k^2\right)-1\right)\right)}{\left(\ln\left(P_{\mathrm{M}}\right)-2\sum_{k=1}^{K}\sigma_k^2\right)\Big/4\sum_{k=1}^{K}\sigma_k^2} \tag{26}$$

As P_{M} goes to infinity, the terms next to $\ln\left(P_{\mathrm{M}}\right)$ can be ignored. Therefore, $\ln\left(P_{\mathrm{M}}\right)$ expressions in the numerator and the denominator cancel each other and (26) reduces to

$$ARDO=\frac{4\sum_{k=1}^{K}\sigma_k^2}{\ln\left(1+\frac{1}{MN}\left(\exp\left(4\sum_{k=1}^{K}\sigma_k^2\right)-1\right)\right)} \tag{27}$$

If we assume that the overall fading variance is small enough, we can use the approximation $\exp\left(x\right)\approx x+1$, which yields

$$ARDO\approx\frac{4\sum_{k=1}^{K}\sigma_k^2}{\ln\left(1+4\sum_{k=1}^{K}\sigma_k^2\Big/MN\right)} \tag{28}$$

As we assumed the overall variance is small enough, we can use the same approximation in its logarithmic form, i.e. $\ln\left(1+x\right)\approx x$, and obtain

$$ARDO\approx\frac{4\sum_{k=1}^{K}\sigma_k^2}{4\sum_{k=1}^{K}\sigma_k^2\Big/MN}=MN \tag{29}$$

3.3 Numerical Results

In this section, we present the numerical results for the outage probability and diversity order of vertical MIMO UVLC links. Unless otherwise stated, we use the simulation parameters in Table II. We consider Pacific Ocean at high latitudes and associated temperature and salinity changes [42] are provided in Figure 3. Scintillation indexes for different layers are computed using the average temperature and salinity values through the layer thickness. The parameters in (4) and (5) that differ from layer to layer are expressed with subscript *k* and computed separately for each layer.

TABLE II. Simulation values

χ_T	1×10^{-6} K^2s^{-3} [53]
ε	1×10^{-2} m^2s^{-3} [53]
λ	0.530 μm
Θ	1
A_k	Computed by TEOS MATLAB Toolbox [54]
B_k	Computed by TEOS MATLAB Toolbox [54]
υ_k	Computed by FVCOM MATLAB Toolbox [55]
D_{T_k}	Computed by FVCOM MATLAB Toolbox [55]
D_{S_k}	$D_{S_k} \approx 0.01 D_{T_k}$ [56, 57]

The change of log-amplitude variance σ_k^2 with respect to depth, based on (4) in conjunction with (5) is shown in Figure 5. Here, d_0 denotes the depth where the transmitter is located, and the x-axis denotes the transmission range. The log amplitude variance for a link in which the transmitter is located in a certain depth d_0 and the transmission range is d_T, is computed by using the average temperature and salinity values, averaged through the considered region and used in (4) and (5). Figure 5.a shows how the log-amplitude variance changes with different depths and transmission ranges (i.e. vertical separation between source and destination). We can observe from the figure that, for the same transmission range, the depth of the source and destination

(i.e. the depth that the transmission is realized) affects the log-amplitude. When we consider the transmission range is fixed to 30 m, we obtain Fig. 3.b, which shows how the log-amplitude variance changes when the source (hence the destination) is located on different depths. We obtain log-amplitude variances of $\sigma_1^2 = 0.0261$, $\sigma_2^2 = 0.0232$, $\sigma_3^2 = 0.0194$, $\sigma_4^2 = 0.0154$ for 30 m links of different source depths starting with sea surface (i.e. 0 m) and going as 30 m, 60 m and 90 m. These are used to model a vertical channel of 120 m distance as four independent turbulence layers. As a benchmark, a hypothetical vertical link with constant turbulence strength also is considered. The constant log-amplitude variance of 0.0892 is computed based on averaging temperature and salinity values over the transmission range of 120 m.

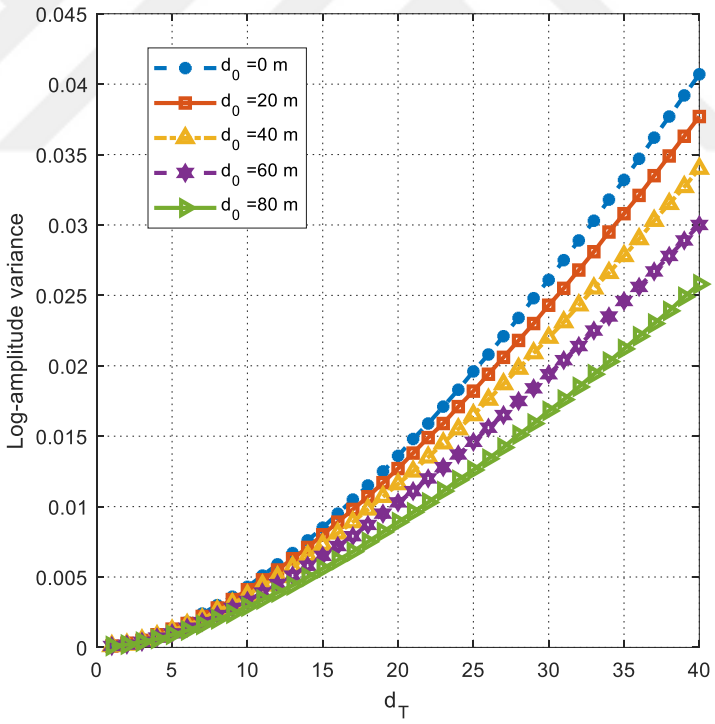

(a)

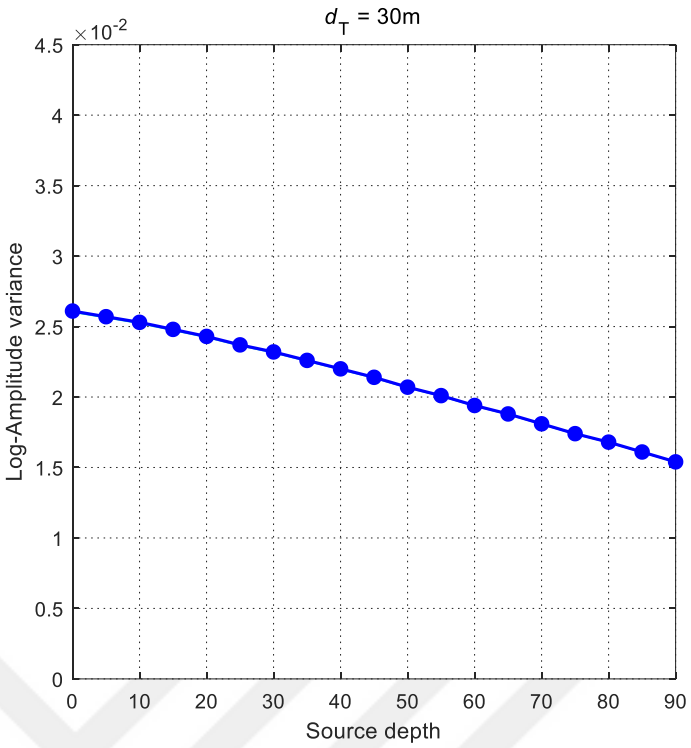

(b)

Figure 5: Change of log-amplitude variance

Figure 6 shows the outage probabilities of MIMO systems with different number of transmit/receive apertures. We consider a transmission range of 120 m. The vertical link is modeled with four layers assuming the same thickness for all layers (i.e., $d_k = 30\text{m}$, $k = 1, \cdots, 4$) [42]. Computed log-amplitude variances that are mentioned previously are used as log-amplitude variances of the independent layers. It can be seen from the figure that the use of multiple apertures provide a considerable performance increase. At a target outage probability of 10^{-6} we observe performance improvements of 3.5 dB, 5.2 dB, and 6.2 dB respectively for $MN = 2$, $MN = 3$ and $MN = 4$ with respect to SISO transmission. As mentioned before, the benchmark hypothetical vertical link with a single variance for 120 m transmission link is also considered. It is observed that such a simplifying assumption (i.e. using a single log-amplitude variance computed by averaging temperature and salinity profiles over 120 m) on the

performance analysis leads to an underestimated outage performance. For instance, if we consider the target outage probability of $P_{\text{out}} = 10^{-6}$, the required power margin in cascade model is 12.70 dB where the constant variance model suggests a power margin of 13.11 dB to achieve the same outage performance for SISO transmission. This difference of 0.41 dB between outage probabilities of two models decrease when the number of transmit/receive apertures increase. Specifically, for $P_{\text{out}} = 10^{-6}$, constant variance model overestimates the outage performance of cascade model by around 0.31 dB, 0.27 dB, and 0.23 dB for $MN = 2$, $MN = 3$ and $MN = 4$ respectively.

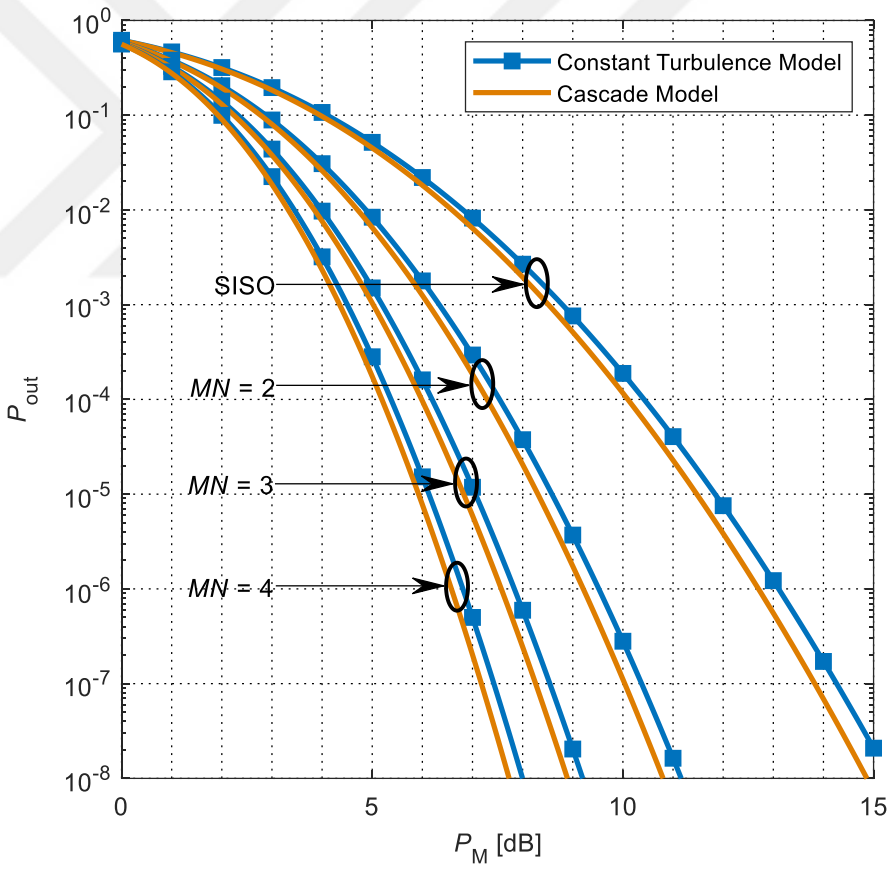

Figure 6: Outage probability of a MIMO UVLC system with different number of transmit/receive apertures for $K = 4$

Figure 7 illustrates the RDO of the UVLC system with for $MN = 2,3,4$ using (22). It can be seen that the RDO converges to the ARDO given by (27). Specifically, ARDO values of 1.86, 2.72, and 3.57 are respectively obtained for $MN = 2,3,4$. It can be readily checked that overall fading variance of 4 layers is $\sigma_T^2 = \sum_{k=1}^{4} \sigma_k^2 = 0.0841$. Since this is not sufficiently small, the convergence of ARDO to *MN* predicted in (29) is not observed here.

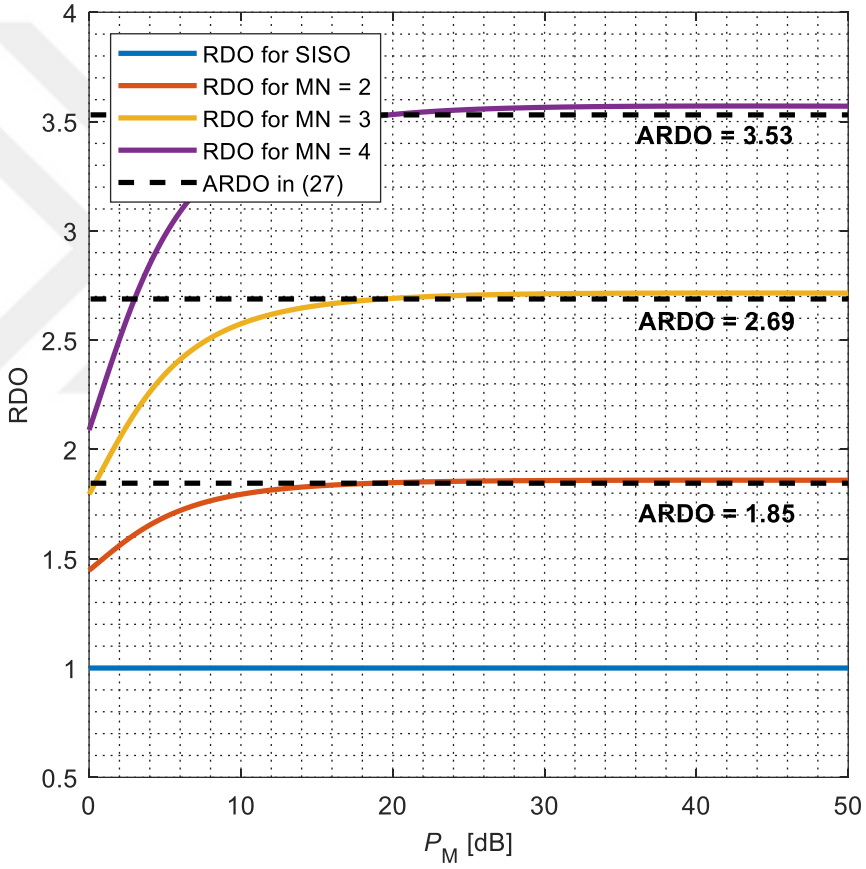

Figure 7: RDO of a MIMO UVLC system with different number of transmit/receive apertures for $K = 4$ layers

In Figure 8, the effect of number of layers is demonstrated. Three different cases, where the number of layers are 3, 4, and 6 are considered for the same total distance of 120 m and $MN = 4$. For the case of four layers, aforementioned log-amplitude variances are

considered. For the cases of three and six layers, the variances are computed using the same temperature and salinity profiles. Computed variances for three layers are, $\sigma_1^2 = 0.0407$, $\sigma_2^2 = 0.0340$, and $\sigma_3^2 = 0.0258$ whereas, for the case of six layers, they are $\sigma_1^2 = 0.0136$, $\sigma_2^2 = 0.0127$, $\sigma_3^2 = 0.0116$, $\sigma_4^2 = 0.0103$, $\sigma_5^2 = 0.0089$, $\sigma_6^2 = 0.0075$. We can see that, as the number of layers increase, the log-amplitude variances of each layer gets smaller. The reason for that is, the thickness of each layer decreases with the increasing number of layers, as the total transmission range is fixed, and the turbulence depends on the distance that the light signal travels. For more layers, the signals will travel a smaller distance for each layer and hence experience a weaker turbulence.

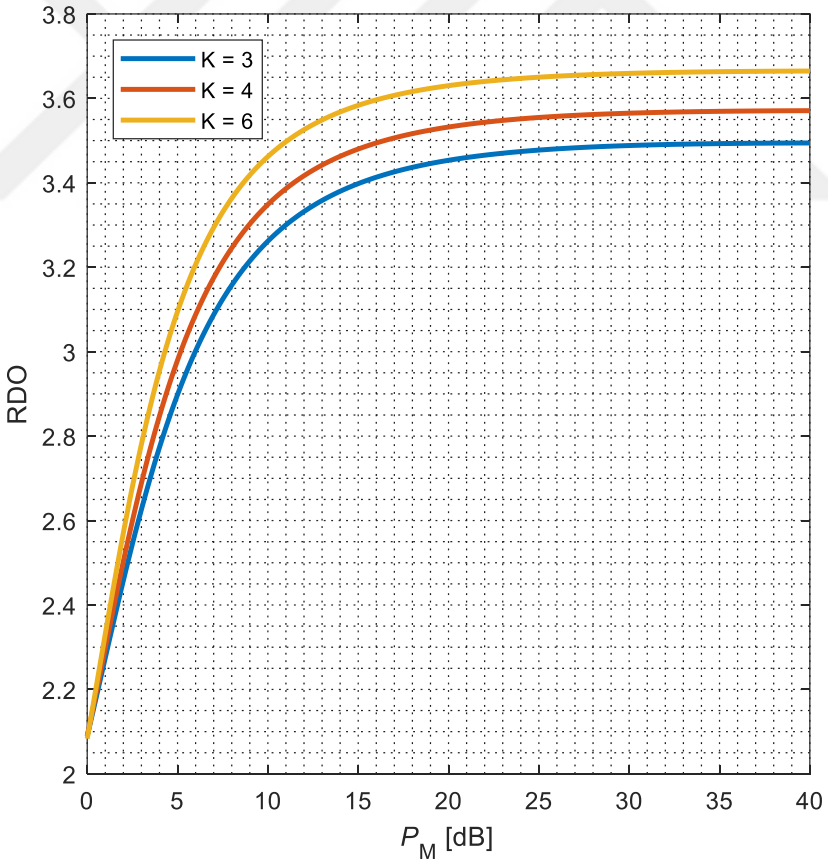

Figure 8: RDO of a MIMO UVLC system with different number of independent turbulence layers for $MN = 4$

We can see from the figure that when the number of layers increase for the same total transmission range, the RDO values converge closer to MN. The explanation of this is the fact that, as the turbulence strengths for individual layers get smaller exponentially with decreasing thickness, even we sum more number of variances, the total variance is smaller. We can directly check this by considering the overall variances for each case, which are 0.0646, 0.0841, and 0.1005 for $K=6$, $K=4$, $K=3$ respectively.

In Figure 9, an unrealistic scenario of 60 layers for 120 m are considered to show that theoretically, the RDO converges to MN, as the variances of each layer are very small and they produce a very small overall variance that satisfies the condition of (29).

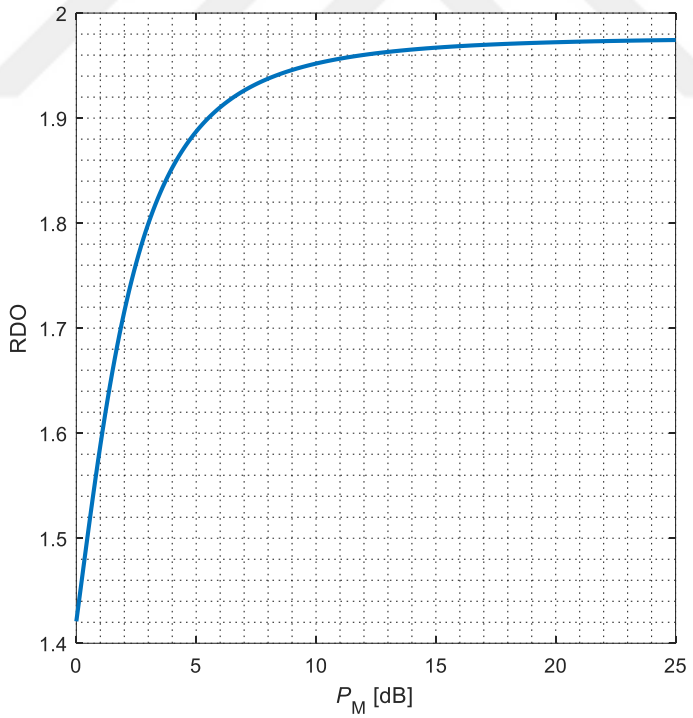

Figure 9: RDO of a MIMO UVLC system with 60 independent turbulence layers for $MN=2$

CHAPTER IV

CONCLUSIONS

Increase in underwater applications of humanity, focused on exploration and data collection, has created a demand for reliable underwater wireless communication systems. Optical wireless communication has offered a great potential to provide reliable systems to satisfy this demand. To be able to achieve that, underwater channel impairments should be investigated, the channel should be comprehensively understood and robust solutions to those impairments should be proposed. To this end, in this thesis we have studied the underwater turbulence, and have provided a quantitative analysis for diversity gain, in vertical MIMO UVLC links. We have provided closed form expressions for the outage probability and the asymptotical relative diversity order, which is a comparative measure for diversity gain. We have done a comparative analysis between SISO, and MIMO schemes with different number of transmit/receive apertures, as well as between vertical cascade channel model and a hypothetical constant turbulence strength channel model.

BIBLIOGRAPHY

[1] M. Uysal and H. Nouri, "Optical wireless communications — An emerging technology," *2014 16th International Conference on Transparent Optical Networks (ICTON)*, Graz, 2014, pp. 1-7.

[2] Z. Ghassemlooy, S. Arnon, M. Uysal, Z. Xu and J. Cheng, "Emerging Optical Wireless Communications-Advances and Challenges," in *IEEE Journal on Selected Areas in Communications*, vol. 33, no. 9, pp. 1738-1749, Sept. 2015.

[3] C. M. Gussen, P. S. Diniz, M. L. Campos, W. A. Martins, F. M. Costa, and J. N. Gois, "A survey of underwater wireless communication technologies," *J. Commun. Inf. Sys.*, vol. 31, no. 1, pp. 242-255, 2016.

[4] Z. Zeng, S. Fu, H. Zhang, Y. Dong and J. Cheng, "A Survey of Underwater Optical Wireless Communications," in *IEEE Communications Surveys & Tutorials*, vol. 19, no. 1, pp. 204-238, Firstquarter 2017.

[5] X. Che, I. Wells, G. Dickers, P. Kear and X. Gong, "Re-evaluation of RF electromagnetic communication in underwater sensor networks," in *IEEE Communications Magazine*, vol. 48, no. 12, pp. 143-151, December 2010.

[6] D. Pompili and I. F. Akyildiz, "Overview of networking protocols for underwater wireless communications," in *IEEE Communications Magazine*, vol. 47, no. 1, pp. 97-102, January 2009.

[7] E. M. Sozer, M. Stojanovic and J. G. Proakis, "Underwater acoustic networks," in *IEEE Journal of Oceanic Engineering*, vol. 25, no. 1, pp. 72-83, Jan. 2000.

[8] S. Jiang, "State-of-the-Art Medium Access Control (MAC) Protocols for Underwater Acoustic Networks: A Survey Based on a MAC Reference Model," in *IEEE Communications Surveys & Tutorials*, vol. 20, no. 1, pp. 96-131, Firstquarter 2018.

[9] S. Q. Duntley, "Light in the sea," *J. Opt. Soc. Amer. A*, vol. 53, pp. 214–233, Feb. 1963.

[10] G. D. Gilbert, T. R. Stoner, and J. L. Jernigan, "Underwater experiments on the polarization, coherence, and scattering properties of a pulsed blue-green laser," in *Proc. SPIE Underwater Photo Opt. I*, vol. 7. Santa Barbara, CA, USA, 1966, p. 3.

[11] The Sonardyne Site. (2016). *Sonardyne International Ltd*. [Online]. Available: http://www.sonardyne.com/products/all-products/instruments/1148-bluecomm-underwater-optical-modem.html

[12] The Ambalux Site. (2016). *Ambalux*. [Online]. Available: http://www.ambalux.com/underwater-transceivers.html

[13] A. M. Căilean and M. Dimian, "Current Challenges for Visible Light Communications Usage in Vehicle Applications: A Survey," in *IEEE Communications Surveys & Tutorials*, vol. 19, no. 4, pp. 2681-2703, Fourthquarter 2017.

[14] D. Karunatilaka, F. Zafar, V. Kalavally and R. Parthiban, "LED Based Indoor Visible Light Communications: State of the Art," in *IEEE Communications Surveys & Tutorials*, vol. 17, no. 3, pp. 1649-1678, thirdquarter 2015.

[15] R. Mesleh, H. Elgala and H. Haas, "On the Performance of Different OFDM Based Optical Wireless Communication Systems," in *IEEE/OSA Journal of Optical Communications and Networking*, vol. 3, no. 8, pp. 620-628, August 2011.

[16] M. Elamassie *et al*., "Effect of eddy diffusivity ratio on underwater optical scintillation index" JOSA A, vol. 34, no. 11, pp. 1969–1973, 2017.

[17] C. D. Mobley *et al.*, "Comparison of numerical models for computing underwater light fields," *Appl. Opt.*, vol. 32, no. 36, pp. 7484–7504, 1993.

[18] C. Wang, H.-Y. Yu, and Y.-J. Zhu, "A long distance underwater visible light communication system with single photon avalanche diode," IEEE *Photon. J.*, vol. 8, no. 5, Oct. 2016.

[19] M. Elamassie, F. Miramirkhani and M. Uysal, "Channel Modeling and Performance Characterization of Underwater Visible Light Communications," *2018 IEEE International Conference on Communications Workshops (ICC Workshops)*, Kansas City, MO, USA, 2018, pp. 1-5.

[20] C. Gabriel, M. A. Khalighi, S. Bourennane, P. Leon and V. Rigaud, "Monte-Carlo-based channel characterization for underwater optical communication systems," in *IEEE/OSA IEEE J. Opt. Commun. Netw*, vol. 5, no. 1, pp. 1-12, Jan. 2013.

[21] F. Akhoundi, J. A. Salehi, and A. Tashakori, "Cellular underwater wireless optical CDMA network: Performance analysis and implementation concepts," *IEEE Trans. Commun.*, vol. 63, no. 3, pp. 882-891, 2015.

[22] M. A. Khalighi, T. Hamza, S. Bourennane, P. Léon and J. Opderbecke, "Underwater Wireless Optical Communications Using Silicon Photo-Multipliers," in *IEEE Photon. J.*, vol. 9, no. 4, pp. 1-10, Aug. 2017.

[23] M. Kong, Y. Chen, R. Sarwar, B. Sun, Z. Xu, J. Han, J. Chen, H. Qin, and J. Xu," Underwater wireless optical communication using an arrayed transmitter/receiver and optical superimposition-based PAM-4 signal," *Optics Express*, Vol. 26, No. 3, pp 3087-3097, Feb. 2018.

[24] Y. Dong, H. Zhang and X. Zhang, "On impulse response modeling for underwater wireless optical MIMO links," *2014 IEEE/CIC International Conference on Communications in China (ICCC)*, Shanghai, 2014, pp. 151-155.

[25] H. Zhang and Y. Dong, ‘‘Impulse response modeling for general underwater wireless optical MIMO links,’’ IEEE Commun. Mag., vol. 54, no. 2, pp. 56–61, Feb. 2016.

[26] W. Liu, Z. Xu, and L. Yang, “SIMO detection schemes for underwater optical wireless communication under turbulence,” Photon. Res., vol. 3, pp. 48–53, Jun. 2015.

[27] Xiang Yi, Zan Li, and Zengji Liu, "Underwater optical communication performance for laser beam propagation through weak oceanic turbulence," Appl. Opt. 54, 1273-1278 (2015)

[28] A. C. Boucouvalas, K. P. Peppas, K. Yiannopoulos and Z. Ghassemlooy, "Underwater Optical Wireless Communications With Optical Amplification and Spatial Diversity," in IEEE Photonics Technology Letters, vol. 28, no. 22, pp. 2613-2616, Nov.15, 15 2016.

[29] H. Gerçekcioğlu, “Bit error rate of focused Gaussian beams in weak oceanic turbulence,” J. Opt. Soc. Am. A 31, 1963–1968 (2014)

[30] S. A. Arpali, Y. Baykal, and Ç. Arpali, “BER evaluations for multimode beams in underwater turbulence,” J. Modern Opt. 63, 1297–1300 (2016)

[31] M. V. Jamali, F. Akhoundi, and J. A. Salehi, “Performance characterization of relay-assisted wireless optical CDMA networks in turbulent underwater channel,” IEEE Trans. Wireless Commun. 15, 4104–4116 (2016)

[32] M. V. Jamali, A. Chizari, and J. A. Salehi, “Performance analysis of multi-hop underwater wireless optical communication systems,” IEEE Photon. Technol. Lett., vol. 29, no. 5, pp. 462–465, Mar. 2017.

[33] T. Shafique, O. Amin, M. Abdallah, I. S. Ansari, M. S. Alouini, and K. Qaraqe, “Performance analysis of single-photon avalanche diode underwater VLC system using ARQ,” IEEE Photon. J., vol. 9, no. 5, pp. 1–11, Oct. 2017.

[34] C. Wang, H. Y. Yu, Y. J. Zhu, and T. Wang, “Blind detection for SPAD-based underwater VLC system under P-G mixed noise model,” IEEE Communications Letters, vol. 21, no. 12, pp. 2602–2605, Dec. 2017.

[35] A. Tabeshnezhad and M. A. Pourmina, “Outage analysis of relay assisted underwater wireless optical communication systems,” Optics Communications, vol. 405, pp. 297–305, Aug. 2017.

[36] K. P. Peppas, A. C. Boucouvalas, and Z. Ghassemloy, “Performance of underwater optical wireless communication with multi-pulse pulseposition modulation receivers and spatial diversity,” IET Optoelectron., vol. 11, no. 5, pp. 180–185, 2017.

[37] M. V. Jamali and J. A. Salehi, "On the BER of multiple-input multiple-output underwater wireless optical communication systems," *2015 4th International Workshop on Optical Wireless Communications (IWOW)*, Istanbul, 2015, pp. 26-30.

[38] M. V. Jamali, J. A. Salehi and F. Akhoundi, "Performance Studies of Underwater Wireless Optical Communication Systems With Spatial Diversity: MIMO Scheme," in *IEEE Transactions on Communications*, vol. 65, no. 3, pp. 1176-1192, March 2017.

[39] M. V. Jamali *et al*., "Statistical distribution of intensity fluctuations for underwater wireless optical channels in the presence of air bubbles," *2016 Iran Workshop on Communication and Information Theory (IWCIT)*, Tehran, 2016, pp. 1-6.

[40] M. V. Jamali *et al*., "Statistical Studies of Fading in Underwater Wireless Optical Channels in the Presence of Air Bubble, Temperature, and Salinity Random Variations," in *IEEE Transactions on Communications*.

[41] Oubei et al, "Simple statistical channel model for weak temperature-induced turbulence in underwater wireless optical communication systems," Optics letters, vol. 42, no. 13, pp. 2455-2458, July,2017.

[42] M. Elamassie and M. Uysal, “Performance characterization of vertical underwater VLC links in the presence of turbulence,” 11th *International Symposium on Communication Systems, Networks & Digital Signal Processing (CSNDSP18)*, Budapest, Hungary, Jul. 2018.

[43] L. C. Andrews and R. L. Phillips, *Laser Beam Propagation Through Random Media*, 2nd ed. Bellingham, WA, USA: SPIE, 2005.

[44] S. G. Wilson, M. Brandt-Pearce, Q. Cao, and M. Baedke, “Optical repetition MIMO transmission with multipulse PPM,” *IEEE J. Select. Areas Commun.*, vol. 23, no. 9, pp. 1901-1909, Sept. 2005.

[45] M. K. Simon and V. Vilnrotter, “Alamouti-type space-time coding for free-space optical communication with direct detection,” *IEEE Trans. Wireless Commun.* vol. 4, no. 1, pp. 35-39, Jan. 2005.

[46] Y. Y. Zhang, H. Y. Yu, J. K. Zhang, Y. J. Zhu, J. L. Wang and X. S. Ji, "On the Optimality of Spatial Repetition Coding for MIMO Optical Wireless Communications," in *IEEE Communications Letters*, vol. 20, no. 5, pp. 846-849, May 2016.

[47] M. Safari and M. Uysal, "Do We Really Need OSTBCs for Free-Space Optical Communication with Direct Detection?," in *IEEE Transactions on Wireless Communications*, vol. 7, no. 11, pp. 4445-4448, November 2008.

[48] E. J. Lee and V. W. S. Chan, "Part 1: optical communication over the clear turbulent atmospheric channel using diversity," in *IEEE Journal on Selected Areas in Communications*, vol. 22, no. 9, pp. 1896-1906, Nov. 2004.

[49] F. Xu, M. A. Khalighi and S. Bourennane, "Impact of different noise sources on the performance of PIN- and APD-based FSO receivers," *Proceedings of the 11th International Conference on Telecommunications*, Graz, 2011, pp. 211-218.

[50] Z. Ghassemlooy, W. Popoola, and S. Rajbhandari, *Optical wireless communications: system and channel modelling with MATLAB*. Boca Raton, FL, USA: CRC Press, 2013.

[51] M. Safari and M. Uysal, "Relay-assisted free-space optical communication," in *IEEE Transactions on Wireless Communications*, vol. 7, no. 12, pp. 5441-5449, December 2008.

[52] M. Safari and M. Uysal, "Cooperative diversity over log-normal fading channels: performance analysis and optimization," in *IEEE Transactions on Wireless Communications*, vol. 7, no. 5, pp. 1963-1972, May 2008.

[53] M. Cheng, L. Guo, J. Li and Y. Zhang, "Channel Capacity of the OAM-Based Free-Space Optical Communication Links With Bessel–Gauss Beams in Turbulent Ocean," in *IEEE Photonics Journal*, vol. 8, no. 1, pp. 1-11, Feb. 2016.

[54] IOC, SCOR and IAPSO, "The international thermodynamic equation of seawater – 2010: Calculation and use of thermodyanmic properties," Intergovernmental Oceanographic Commission, Manual and Guides UNESCO (English), No. 56, 2010.

[55] Chen *et al.*, An Unstructured-grid, Finite-volume Community Ocean Model: FVCOM User Manual. Sea Grant College Program, Massachusetts Institute of Technology, 2012.

[56] John H. Steele, Steve A. Thorpe and Karl K. Turekian, *A derivative of the Encyclopedia of Ocean Sciences: Elements of Physical Oceanography*. Elsevier, 2010.

[57] L. Goodman and M. M. S.-Córdova. "On observing acoustic backscattering from salinity turbulence." J. Acoust. Soc. Am., vol. 130, no. 2, pp. 707-715, 2011.

VITA

Anıl Yılmaz was born in Istanbul, Turkey, on August 7, 1992. He received his B.Sc. from Özyeğin University in Electrical & Electronics Engineering in 2015. He is currently a M.Sc. student in Özyeğin University, working with Professor Murat Uysal. His main research interests include visible light communication, and underwater optical wireless communications.